nature climate change

SUPPLEMENTARY INFORMATION

https://doi.org/10.1038/s41558-018-0356-x

In the format provided by the authors and unedited.

Increased snowfall over the Antarctic Ice Sheet mitigated twentieth-century sea-level rise

B. Medley[1]* and E. R. Thomas[2]

[1]Cryospheric Sciences Laboratory, NASA Goddard Space Flight Center, Greenbelt, MD, USA. [2]British Antarctic Survey, Cambridge, UK.
*e-mail: brooke.c.medley@nasa.gov

Increased snowfall over the Antarctic Ice Sheet mitigated 20th century sea level rise

Authors: B. Medley[1†] and E.R. Thomas[2]

Affiliations:

[1]NASA Goddard Space Flight Center, Cryospheric Sciences Laboratory, Greenbelt, MD 20771, USA.

[2]British Antarctic Survey, Cambridge, UK CB3 0ET.

[†]Correspondence to: brooke.c.medley@nasa.gov.

Supplementary Methods

Supplementary Figures

Supplementary Figure S1 | Ice core locations.

Supplementary Figure S2 | Number of ice cores as a function of time used in the reconstruction.

Supplementary Figure S3 | Magnitude bias of the reanalysis precipitation-minus-evaporation products.

Supplementary Figure S4 | Validation statistics of the full reconstruction in comparison to the 53 ice-core records for the three reanalysis-based reconstructions.

Supplementary Figure S5 | Correlation coefficients between the 1980-2000 MERRA-2 time series and the ice-core records and $R_{MERRA\text{-}2}$ reconstruction.

Supplementary Figure S6 | Cross-validation statistics of reconstructed trends at each of the 53 ice-core sites and over different time intervals for reconstructions using CFSR, MERRA-2, and ERA-Interim.

Supplementary Figure S7 | Comparison of the sea-level mitigation from the full reconstruction with several alternate reconstruction scenarios.

Supplementary Figure S8 | Maximum correlation coefficient for each grid cell with the MERRA-2 *P–E* records using four different ice-core distributions.

Supplementary Figure S9 | Cross-validation statistics of temporally independent reconstructed trends at each of the 53 ice-core sites and the 27 Zwally drainage basins for reconstructions using CFSR, MERRA-2, and ERA-Interim.

Supplementary Figure S10 | Comparison of the 1957–2000 SAM-Congruent trends and the reconstructed trends using the three different reanalyses.

Supplementary Tables

Supplementary Table S1 | Ice-core records used in the reconstruction

Supplementary Table S2 | Mean and median validation statistics for each reanalysis-based reconstruction.

Supplementary Table S3 | Area-weighted and accumulation-weighted mean proportion of variance explained for different sectors and time slices.

Supplementary Table S4 | Total sea-level mitigation by 2000 for the three reconstructions under various scenarios.

Supplementary Table S5 | The reconstructed and SAM-congruent 1957–2000 trends and their residual by sector.

Supplementary Methods: Reconstruction Validation

To ensure that our reconstructions are robust representations of the ice-core records, we evaluate several skill statistics as performed by other reconstructions of Antarctic atmospheric pressure[1] and air temperature[2]: explained variance (R^2), root-mean-square error (RMSE), reduction of error (RE), and coefficient of efficiency (CE). Because change is of importance, we also evaluate the absolute errors in trends (AE). All statistics (Supplementary Fig. S4; Supplementary Table S2) are based on comparison of the relative (not absolute) reconstructed time series with the original ice-core record to avoid bias based on the large spread in the mean annual accumulation. Thus, an RMSE of 0.2 indicates the annual reconstruction is largely within 20% of ice-core record (The median RMSE of R_{MERRA2} is 0.19). The RE and CE can range from negative infinity to one, and values above zero suggest that the reconstruction is more valid than using the climatological mean. We find that all three models perform well and are not visibly differentiable (Supplementary Fig. S4), but we note that R_{MERRA2} has the highest average skill in nearly every category whether the mean or median is used. Combining its higher performance with the fact that MERRA-2 $P–E$ is the least biased, R_{MERRA2} is the most robust reconstruction.

We further complete several additional cross-validation reconstructions to ensure that the results are robust. Specifically, we investigate the impact of slight modifications to our methodology or observations on the reconstructed trends, which are of the most importance when assessing the impacts of SA change on GMSL. We describe each of the cross-validation reconstructions below:

1. *JackCore*: We create 53 alternative reconstructions where each ice-core record is removed in a jackknife fashion, resulting in cross-validation reconstructions based on a subset of 53 records. This evaluator set allows us to determine whether the results are strongly influenced by one or more records and if our observation data set is comprehensive enough. The *DropCore*

evaluation uses a subset of these 53 reconstructions. Specifically, it only compares the unused record with the reconstruction from which its excluded.

2. *RemoveSAM*: A single cross-validation reconstruction that uses a modified reanalysis *P*−*E* time series that has the SAM-congruent signal removed. Prior to reconstruction, we calculate the SAM index[3] for each reanalysis, and determine the cell-by-cell sensitivity to the SAM using linearly detrended time series, which is used to remove the SAM-congruent signal from the reanalysis *P*−*E.* Spatial weights in the reconstruction are next determined using this SAM-removed reanalysis. We can then ensure that our results are not trained to mimic the SAM-congruent signal if it happens to be unrealistically strong within a given reanalysis.
3. *ComplCores*: Under this cross-validation scenario, we create a single reconstruction that uses only a subset of the ice-core records: specifically, only those which span the entire 1801−2000 interval. Thus, only 16 records are employed (Supplementary Fig. S8). Using this evaluator data, we can assess whether our full reconstruction contains large artifacts due to an evolving ice-core distribution with time. Large areas of the EAIS and the AP are not sufficiently resolved in this reconstruction.
4. *JackYear*: Similar to the *JackCore* cross-validation, we create 38 (37 for R_{MERRA2}) reconstructions that are generated by removing each year (and the two neighboring years) from the reanalysis *P*−*E* time series. The spatial signatures are then assessed using this modified reanalysis data set. Here, we test whether our 37/38-year "calibration" window is sufficient to capture most of the spatiotemporal patterns of SA over the AIS. If removal of a year from the *P*−*E* time series results in a significant departure from the full reconstruction, we would have to question whether the latter was robust.
5. Adj_{core} *and* Adj_{model}: Here, we investigate the potential impact of an evolving ice-core array through time by creating an adjustment time series for each grid cell. The Adj_{core} correction is

determined by rerunning the reconstruction over the interval common to all ice cores (1952–1988) under every ice-core combination throughout the entire 200-year interval. The difference between the time series from the full ice-core array and each combination of cores potentially informs us about the bias imposed on our full reconstruction as the ice-core network evolves through time. The final Adj_{core} reconstruction uses the original reconstruction and corrects for the aforementioned adjustment. The Adj_{model} reconstruction is generated as above except using the reanalysis *P*–*E* timeseries at each core site rather than the ice-core record. The common interval is thus 1979/80-2016.

In total, we generated 95 R_{MERRA2} and 96 R_{CFSR} and R_{ERAI} cross-validation reconstructions, which when combined with the full reconstructions amounts to a total of 290. The cross-validation reconstructions are compared to the full reconstruction to assess the durability of our results. Specifically, we evaluate the differences in trends at each of the 53 ice-core sites in Supplementary Fig. S6, where we regress the full trends against the cross-validation trends at each site. Thus, values close to unity suggest a robust reconstruction.

Like the validation skill statistics, we find that all three reconstructions perform well (Supplementary Fig. S6). The largest deviations from the full reconstruction occur in the *ComplCore* comparison, which is expected since it uses data from only 16 records; however, they generally span unity. Removing the SAM-congruent signal, individual years, and/or ice-core records from our reconstruction does not significantly change our results (Supplementary Fig. S7; Supplementary Table S4).

We next build a 1979/80–2000 time series that is independent of the reanalysis *P*–*E* from that year. This scenario is accomplished by combining the reconstructed SA for the year that had been eliminated in the *JackYear* cross-validation reconstructions (e.g., annual values for 1980 are taken from the *JackYear* reconstruction where 1980 was removed, and so on). We then correlate this temporally-independent reconstruction with the full reconstruction at each of the 53 core sites as well as for each of the 27

drainage basins (Supplementary Fig. S9). The two reconstructions strongly relate; thus, the calibration time window is sufficiently long.

Next, we evaluate how our estimates of 20th century sea-level mitigation vary under the various cross-calibration reconstructions (Supplementary Fig. S7). Only the R_{MERRA2} cross-validation results are displayed; however, the results from R_{CFSR} and R_{ERAI} are not sufficiently different. We plot the both the non-bias-corrected and bias-corrected curve as well, which essentially fall on top of the one another. The pale red and blue lines signify each of the 53 *JackCore* and 37 *JackYear* cross-validation reconstructions, respectively, and their average is in bold, which predictably fall on top of the full reconstruction. We find that manipulations to our methodology do not significantly impact our results, and that the spread of possible outcomes falls well within our uncertainties. Notably, using only the 16 complete records would result in more sea-level mitigation, whereas removal of the SAM-congruent trend prior to reconstruction does not impact our results. The largest deviations from the full reconstruction occur when excluding an ice-core record and, to a lesser extent, removing years from the calibration interval. Undoubtedly, removal of a record from a site that is isolated from the others will result in a major difference

The Adj_{core} and Adj_{model} scenarios act to reduce and increase sea-level mitigation, respectively. Specifically, the area-weighted mean absolute corrections under the Adj_{core} scenario are merely 1.3% (ERA-Interim), 1.2% (MERRA-2), and 1.1% (CFSR) for the entire AIS where only values outside of the contemporaneous 1952–1988 interval are used. The standard error of the mean ($\sigma/\sqrt{n}$) of the ice-core records over the 1952–1988 range from 1–7% (median = 4%), which suggests that the contemporaneous ice-core interval is not sufficiently long to distinguish with confidence whether the correction is real or simply an artifact of the short 37-year interval of comparison. Similarly, the standard error of the mean of the reanalysis *P*–*E* timeseries at the ice-core locations between 1980 and 2016 range from 2–12%

(median = 3%), indicating that use of the 37-year reanalysis time interval under the Adj_{model} scenario is not enough either. Thus, we include both scenarios as alternative reconstruction scenarios (Supplementary Fig. S7; Supplementary Table S4), but we are limited in their interpretation due to the short time interval for comparison, and thus large errors, in conjunction with the relatively low (1.1–1.3%) typical adjustment values. These limitations combined with the fact that the two scenarios result in opposing changes suggests interpretation of their impact as significant is tenuous, yet we acknowledge that we might lack the data necessary for evaluation.

Supplementary Figures

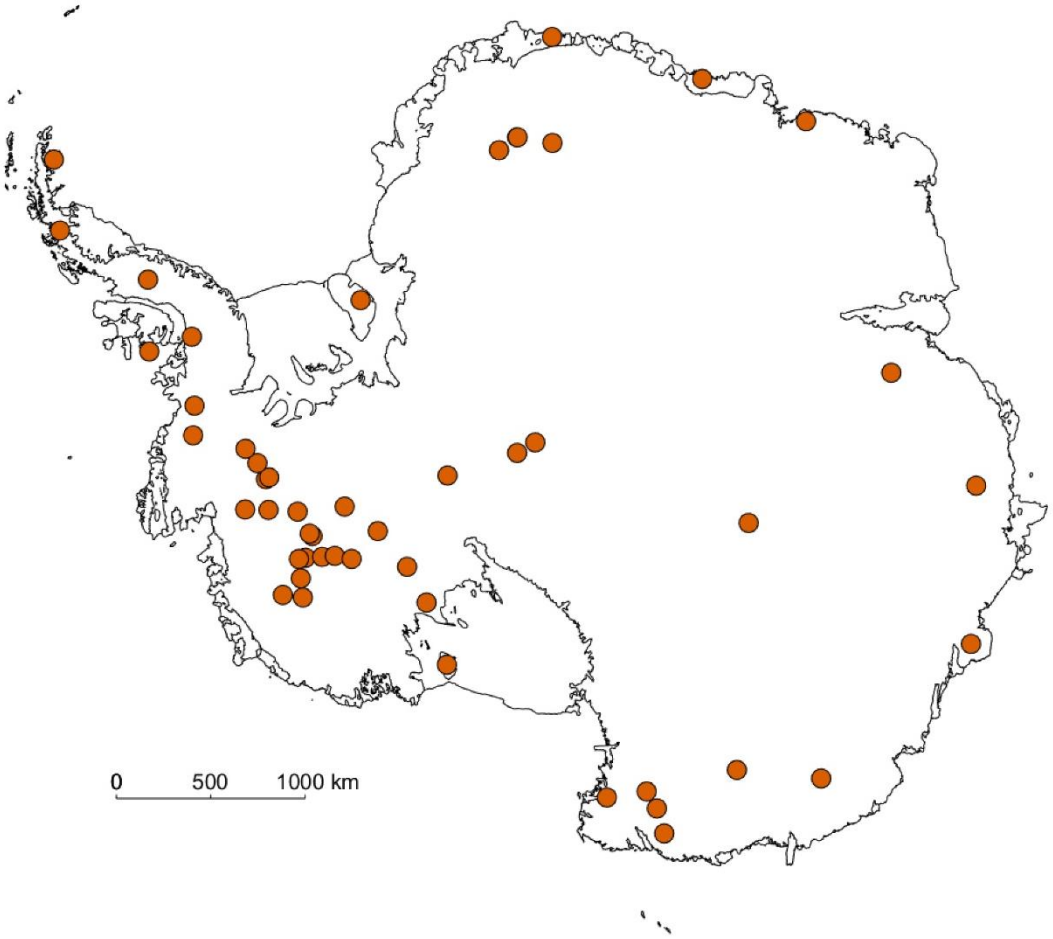

Supplementary Figure S1 | Ice core locations. Locations of the 53 ice cores used in the reconstruction and listed in Supplementary Table 1.

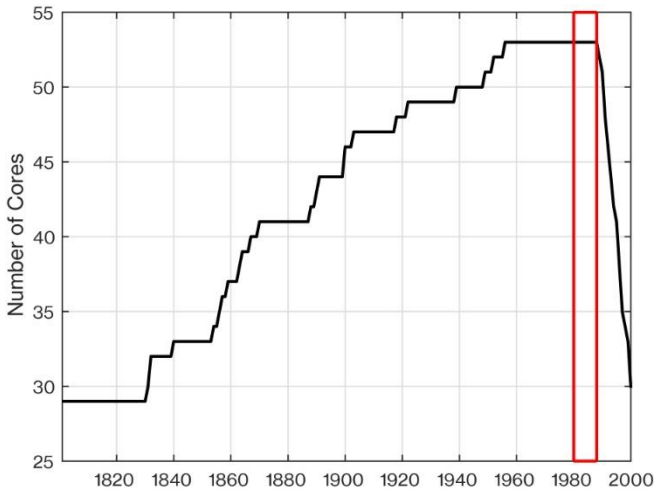

Supplementary Figure S2 | Number of ice cores as a function of time used in the reconstruction. The red box represents the baseline interval (1980-1988) used to relate the ice-core records with the reanalysis *P*−*E*. Only sixteen records exist that span the entire 200-year interval.

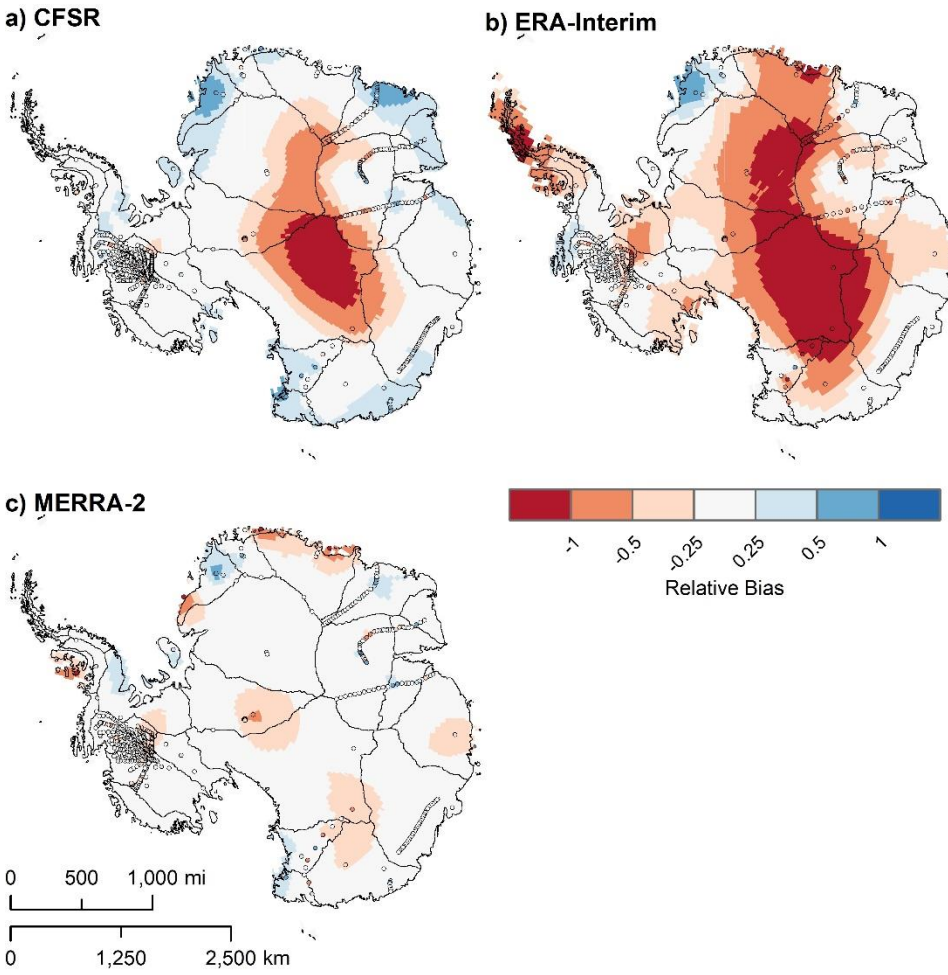

Supplementary Figure S3 | Magnitude bias of the three reanalysis precipitation-minus-evaporation products. Kriged mean annual *P–E* bias for **a**, CFSR, **b**, ERA-Interim, and **c**, MERRA-2 based on several observations. The bias values that form the basis of the final kriged product are enclosed by a black circle. Blues indicate the model is overestimating *P–E*, while reds suggest underestimation. The atmospheric reanalysis *P–E* values exhibit biases in total magnitude across much of the AIS and vary substantially from one another[4]. We evaluate the magnitude bias using observations of contemporaneous annual values of surface mass balance from both the ice-core data presented in Supplementary Table 1 as well as radar-derived measurements over the Pine Island and Thwaites glacier catchments[5] and an AIS-wide data base of surface mass balance[6]. Although it limited spatial coverage, we only used observations from the latter that fell within (and only within) the reanalysis period (1979/80-2016). The surface mass balance values were then compared to the modeled *P–E* from the grid cell to which they belong for the contemporaneous years, $bias = (model - observation) / model$. If multiple observations exist for a single grid cell, all the observations are averaged together to create one bias correction value per grid cell. In such a manner, we found the relative error in the modeled *P–E* magnitudes, which were then interpolated over the entire AIS using the statistical interpolation method of kriging (i.e., distance-based interpolation).

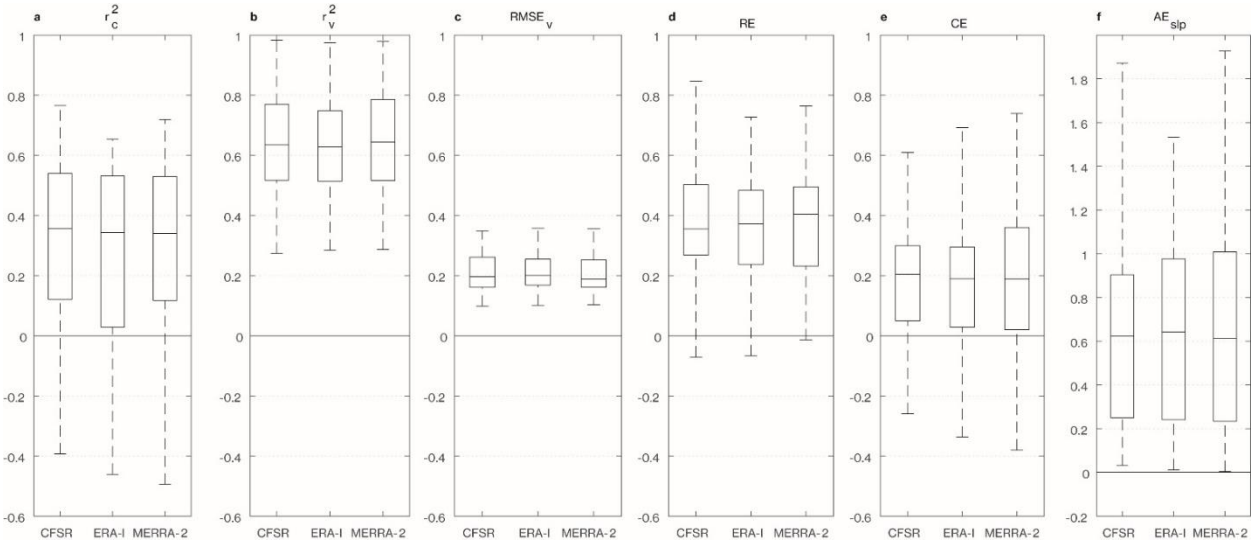

Supplementary Figure S4 | Validation statistics of the full reconstruction in comparison to the 53 ice-core records for the three reanalysis-based reconstructions. All boxes represent the upper and lower quartiles, the median slices the box in half, and the whiskers show the limits of the distribution. We evaluate (a) the proportion of explained variance over the calibration (1980-88) interval, 'r^2_c', (b) the squared Pearson correlation coefficient over the verification (1801-1979; 1989-2000) interval, 'r^2_v', (c) the root-mean-squared error (in relative percent) over the verification interval, '$RMSE_v$', (e) the reduction of error over the verification interval, 'RE', (f) the coefficient of efficiency over the verification interval, 'CE', and (f) the absolute error in trends (in percent per decade) over the entire interval, 'AE_{slp}', between the actual ice-core record and the reconstructed value. Values nearest to 1 for r^2_c, r^2_v, RE, and CE indicate a more robust representation of the observations, are ordered by increasing rigorousness, and are defined in ref.[7]. For RE and CE, values above 0 indicate the reconstruction during the verification interval has higher skill than use of the calibration and verification climatology, respectively. Values close to 0 for the $RMSE_v$ and AE_{slp} suggest the reconstruction is capable of preproducing the observed variability and trends with skill.

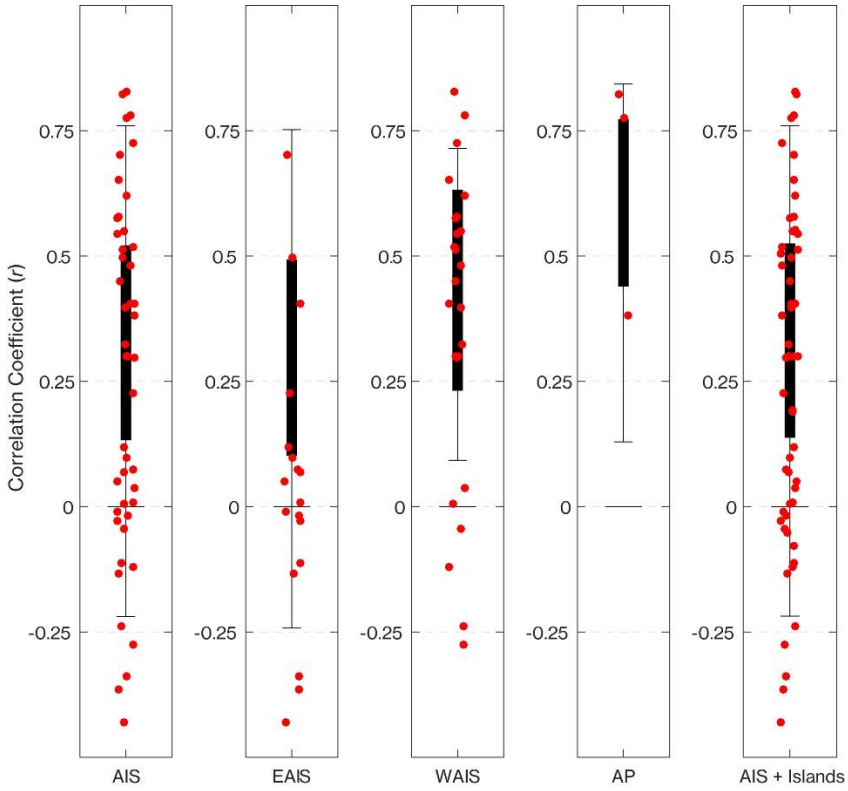

Supplementary Figure S5 | Correlation coefficients (*r*) between the 1980-2000 MERRA-2 time series and the ice-core records (red dots) and $R_{MERRA\text{-}2}$ reconstruction (black box and whiskers). The correlations with the reconstruction are calculated on a grid cell-by-grid cell basis, and the distributions presented are weighted by area. The whiskers represent the 95% bounds by area, and the black bar spans the upper (75%) and lower (25%) quartiles by area. Because the ice-core records provide the time-series basis of the reconstruction, both correlation distributions span similar ranges. Even though several cores are negatively correlated with the reanalysis, the reconstruction typically performs better, especially for WAIS and EAIS, which suggests that the use of multiple cores helps minimize the impact of small-scale variability (glaciological noise). It is not surprising that several ice cores are negatively correlated, especially over the EAIS, since (1) the time interval in common is relatively short (9-21 years) and (2) the signal to noise ratio is very low in low accumulation regions. Thus, the interannual variability might suffer somewhat, but the long term-trends are robust. The values for the same comparison with R_{ERAI} and R_{CFSR} are very similar.

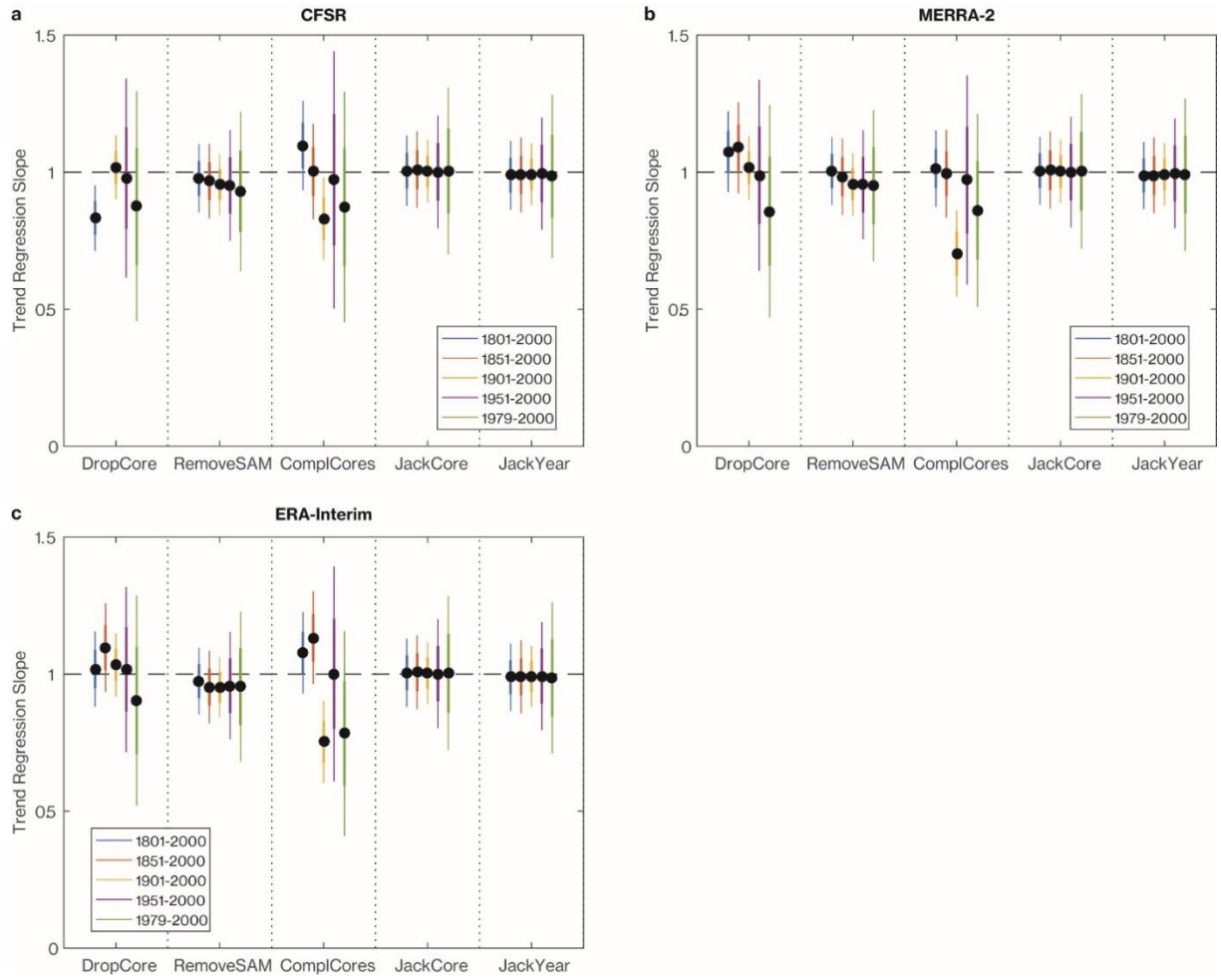

Supplementary Figure S6 | Cross-validation statistics of reconstructed trends at each of the 53 ice-core sites and over different time intervals for reconstructions using a, CFSR, b, MERRA-2, and c, ERA-Interim. We compare the reconstructed trends at the ice-core sites under a series of alternate reconstructions to the full reconstruction to ensure robustness in our results. 'DropCore' represents a series of 53 reconstructions whereby each ice-core record was dropped one-by-one, generating reconstructed time series that are independent from the record itself. The values presented represent the regression slope between the independent dropped site reconstructed trends and the full reconstruction. The thick and thin vertical bars represent the 1- and 2-sigma trend bounds. 'RemoveSAM' is a single reconstruction whereby the SAM-congruent signal in the reanalysis time series is removed. 'ComplCores' is a single reconstruction that uses only the 16 ice-core records that are complete over the full 1801-2000 time period (see Supplementary Figure 5b to see limitations). 'JackCore' is the same 53 alternate reconstructions from 'DropCore' but all sites are compared (rather than only the independent records). The latter allowed us to see whether inclusion of one or a few records had a major influence on our results. 'JackYear' represents a series of 37 (MERRA-2) or 38 (CFSR, ERA-Interim) subsets of the reanalysis time series used for generating the weights by removing one year at a time (along with the 2 neighboring years) from the reanalysis record and reconstruct accumulation rates. The latter ensures that length of the reanalysis record is long enough to ensure that one or a few strong atmospheric events do not bias our results. Robust trends should fall close to unity for all alternate reconstructions.

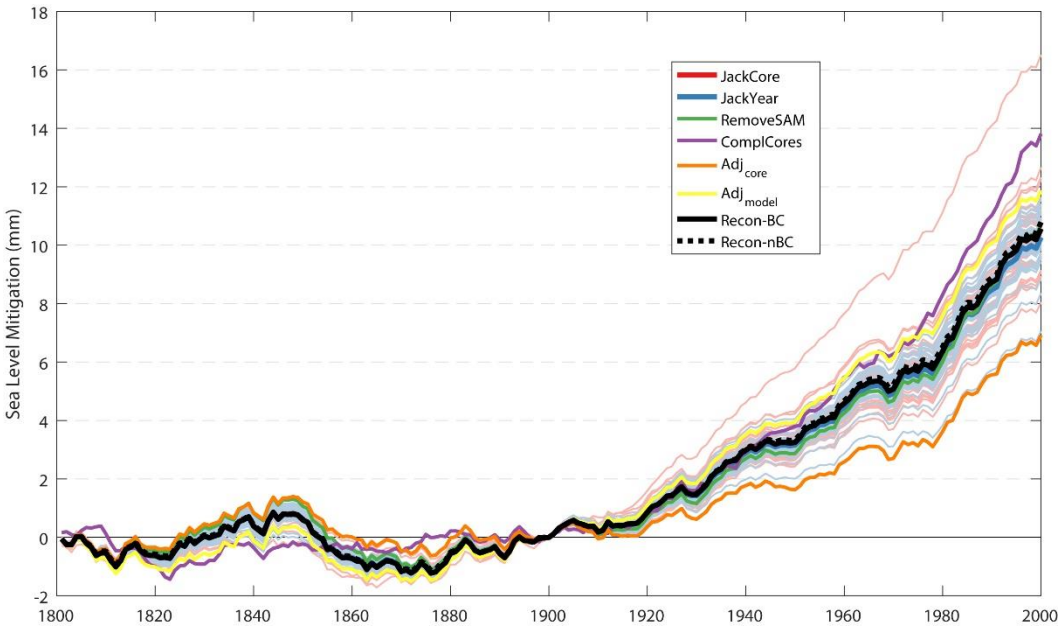

Supplementary Figure S7 | Comparison of the sea-level mitigation from the full reconstruction with several alternate reconstruction scenarios. The pale red lines represent 53 alternate reconstructions where a single ice-core record is removed, and the bold red line is the mean. The pale blue lines represent the 37 alternate reconstructions where a single year (and its two neighbors) are removed from the reanalysis prior to derivation of weights, and the bold blue line is the mean. The bold green line is the single reconstruction where the SAM-congruent P-E signal was removed from the reanalysis time series prior to derivation of weights. The bold purple line is the single reconstruction that uses only the 16 ice-core records that are complete over the 1801-2000 time period. The bold black line is the reconstruction using bias corrected reanalysis values, and the dashed black line is the full reconstruction using the non-bias corrected reanalysis data. MERRA-2 is our model of choice because the model exhibits the least magnitude bias of the three models.

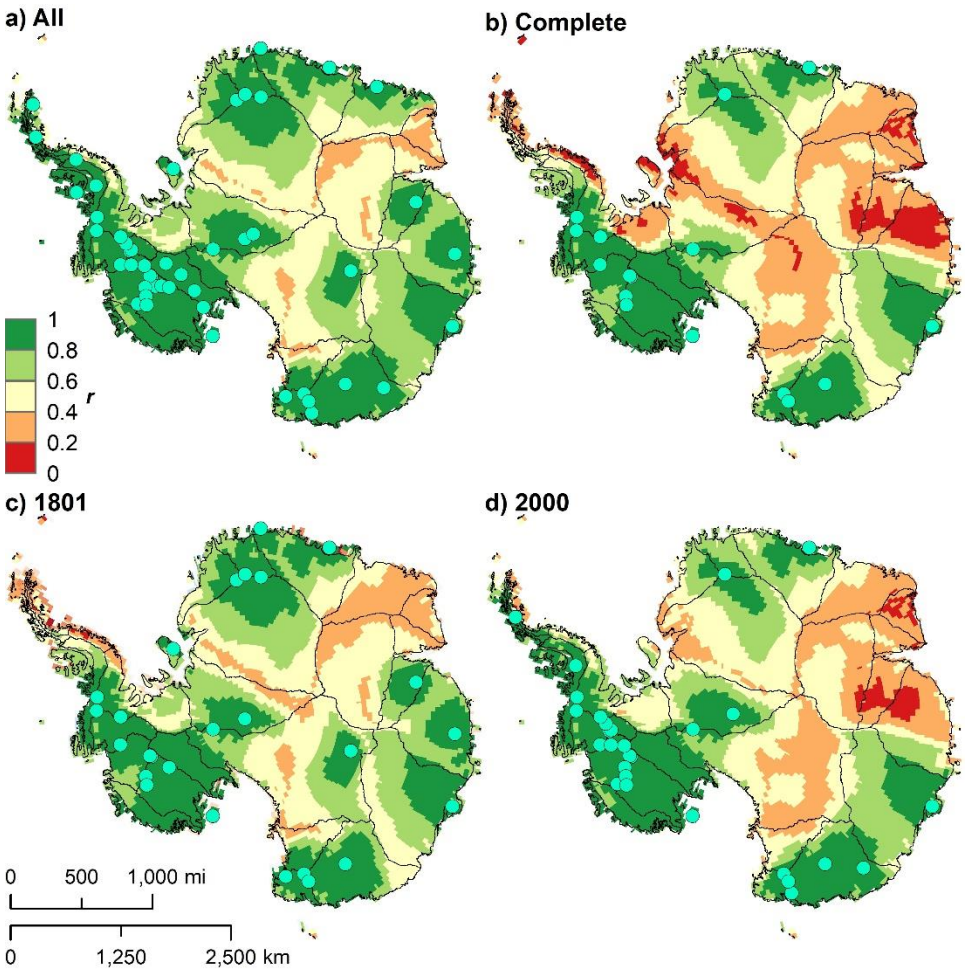

Supplementary Figure S8 | Maximum correlation coefficient for each grid cell with the MERRA-2 *P–E* records using four different ice-core distributions (circles). The correlation values provide the basis of the weighting scheme for the reconstruction; however, the number of ice cores varies in time, so here we present four different maximum correlations using different ice core distributions: **a**, all 53 sites, **b**, the 16 sites with records that span the entire 1801–2000 time interval, **c**, the sites with records covering the first year of the reconstruction (1801), and **d**, the sites with records covering the final year of the reconstruction (2000). The same plots were made with ERA-Interim and CFSR, which both show nearly identical results, but are not included.

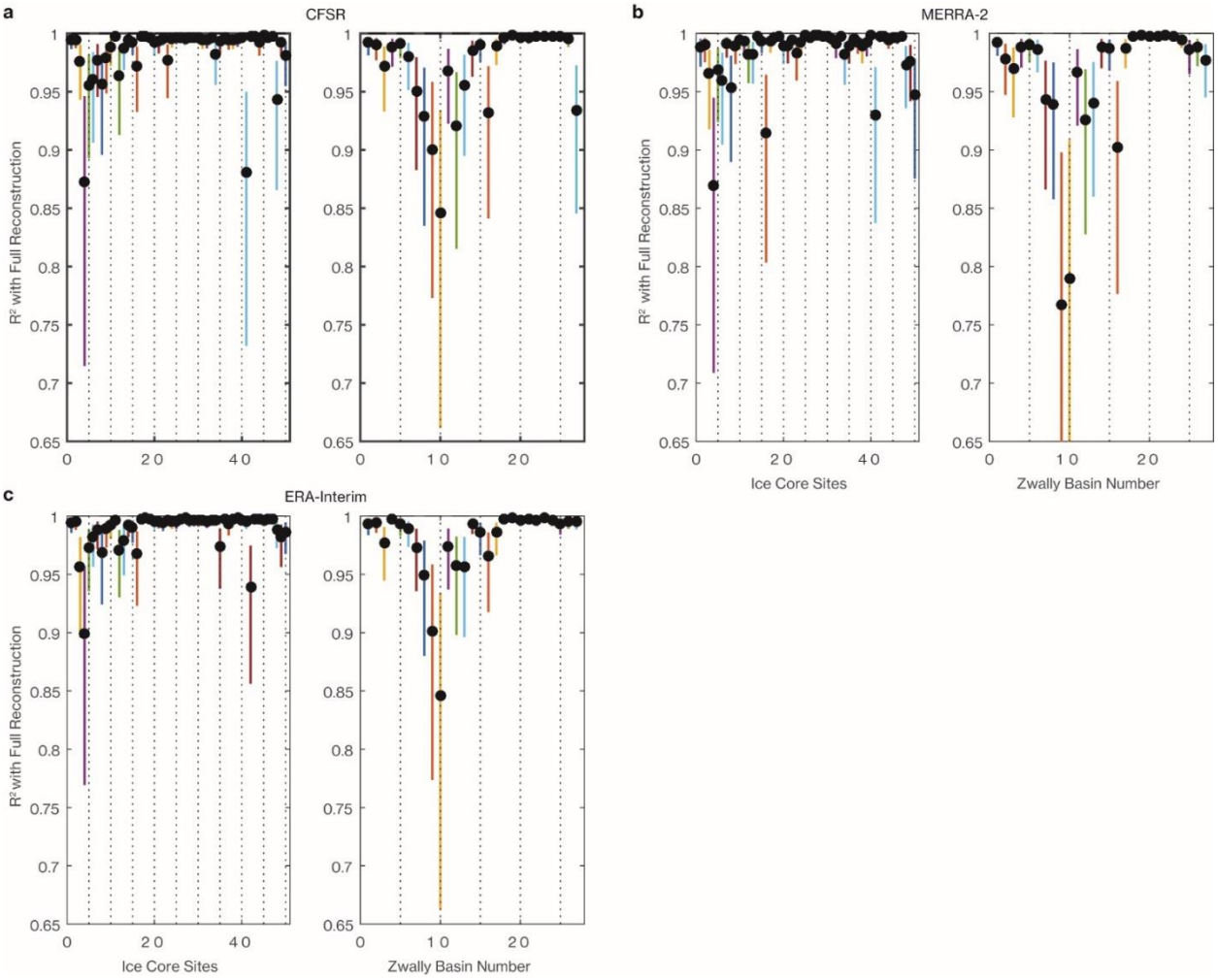

Supplementary Figure S9 | Cross-validation statistics of temporally independent reconstructed trends at each of the 53 ice-core sites and the 27 Zwally drainage basins for reconstructions using a, CFSR, b, MERRA-2, and c, ERA-Interim. Using the 21/22 of the 'JackYear' alternate reconstructions covering 1979/80-2000, we generate a single reconstruction by concatenating the values from the reconstruction that is independent of that year (i.e., combine the 1980 values from the 1980 'JackYear' reconstruction with the 1981 values from the 1981 'JackYear' reconstruction, and so on). Each year in this reconstruction is not derived from reanalysis data from that year for weighting. This temporally independent alternate reconstruction is correlated with the full reconstruction at each of the ice-core sites as well as over area-integrated basins. The vertical lines represent the 95% confidence bounds.

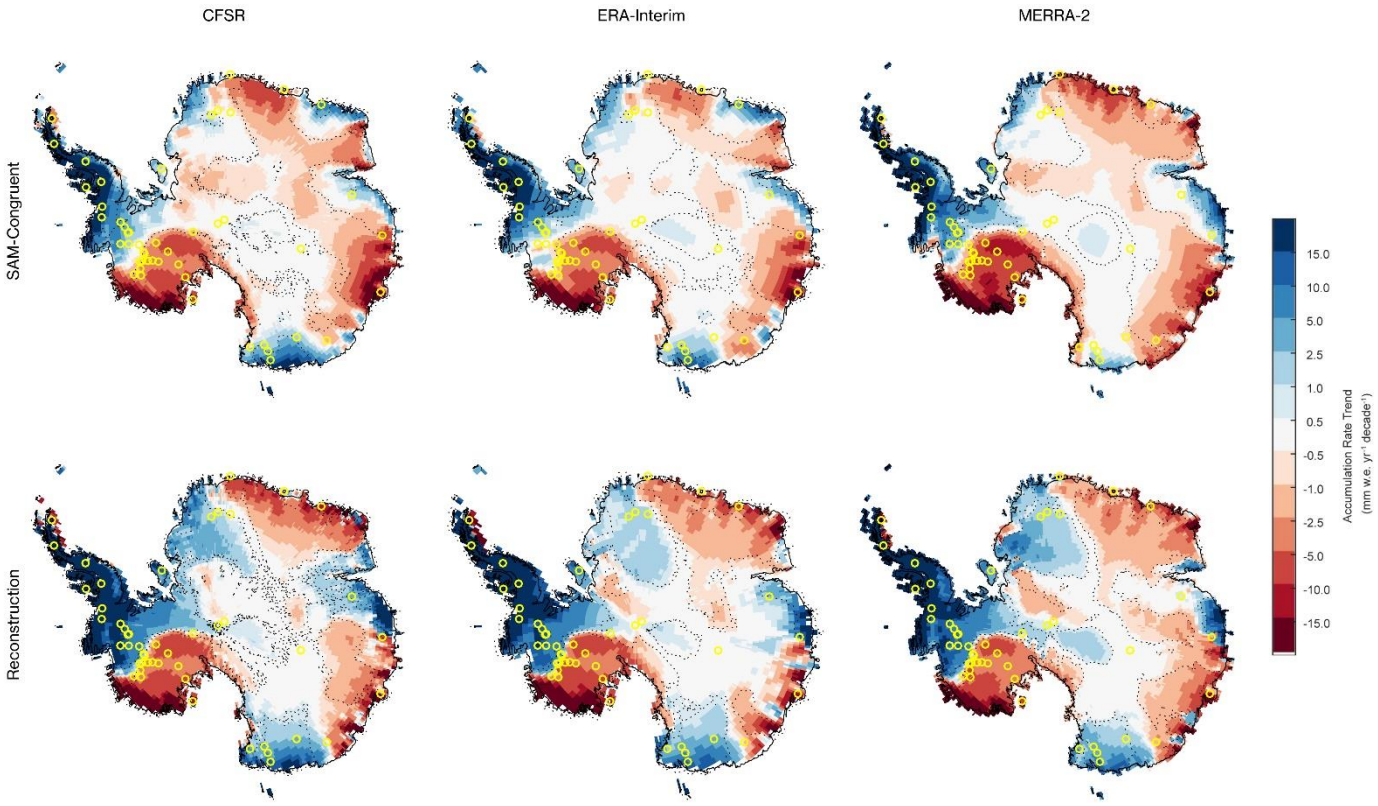

Supplementary Figure S10 | Comparison of the 1957–2000 SAM-Congruent trends and the reconstructed trends using the three different reanalyses. The upper maps display the SAM-congruent trend while the lower plots contain the reconstructed trend. The left, middle, and right columns refer to the reanalysis model used: CFSR, ERA-Interim, and MERRA-2, respectively. The ice cores used in the reconstruction are displayed yellow open circles.

Supplementary Tables

Supplementary Table S1 | Ice-core records used in the reconstruction

Name	Lat (°)	Lon (°)	Elev	Time Interval
Vostok composite	-78.47	106.83	3488	1654-2010
B31Site DML07[9]	-75.58	-3.43	2680	1000-1994
B32Site DML05[9]	-75	-0.01	2892	1248-1996
B33Site DML17[9]	-75.17	6.5	3160	1250-1997
South Pole 1995[10]	-90	0	2850	1801-1991
D66[11]	-68.94	136.94	2333	1864-2003
LGB65[12]	-71.85	77.92	1850	1745-1996
GV2[11]	-71.71	145.26	2143	1670-2003
US-ITASE-2002-7[13]	-88.9989	59.9744	3000	1900-2002
US-ITASE-2002-4[13]	-86.5	-107.99	2586	1594-2003
DSS Law Dome[14]	-66.77	112.807	1370	-22-1995
200th km[15]	-68.25	94.08	1990	1640-1988
Berkner Island (South)[16]	-79.57	-45.72	890	1000-1992
Gomez[17]	-73.59	-70.36	1400	1858-2006
James Ross Island[18]	-64.22	-57.68	1640	1832-1997
Dyer Plateau[19]	-70.68	-64.87	2002	1505-1988
Bruce Plateau[20]	-66.038	-64.078	1975.5	1900-2009
Beethoven[21]	-71.9	-74.6	580	1949-1991
Ferrigno[22]	-74.57	-86.9	1354	1703-2010
Bryan Coast[22]	-74.496	-81.678	1177	1712-2010
DIV2010[23]	-76.77	-101.74	1330	1786-2010
THW2010[23]	-76.95	-121.22	2020	1867-2010
PIG2010[23]	-77.96	-95.96	1590	1918-2010
WDC05A[24]	-79.46	-112.09	1806	1775-2005
WD05Q[24]	-79.46	-112.09	1759	1522-2005
WAIS 2014[25]	-79.46	-112.09	1759	2006-31ka
CWA-A[26]	-82.3671	-119.2855	950	1939-1993
CWA-D[26]	-81.3723	-107.275	1930	1952-1993
Siple dome-94[27]	-81.648077	-148.79	620	1891-1994
Upstream-C (UP-C)[27]	-82.43911	-135.97195	525	1870-1996
Ross ice drainage	-78.73	-116.33	1740	1831-1995
Ross ice drainage	-79.46	-118.05	1603	1922-1995
Ross ice drainage	-80.01	-119.43	1530	1903-1995
US-ITASE-1999-1[27]	-80.62	-122.63	1350	1724-2000
US-ITASE-2000-1[27]	-79.3838	-111.24	1791	1673-2001
US-ITASE-2000-3[13]	-78.433	-115.9172	1742	1971-2001
US-ITASE-2000-4[27]	-78.0829	-120.0764	1697	1798-2000
US-ITASE-2000-5[27]	-77.683	-123.995	1828	1718-1999
US-ITASE-2001-1[13]	-79.1597	-104.9672	1842	1986-2002
US-ITASE-2001-2[27]	-77.8436	-102.9103	1746	1892-2002
US-ITASE-2001-3[27]	-78.1202	-95.6463	1620	1858-2002
US-ITASE-2001-4[13]	-77.6116	-92.2483	1483	1986-2001
US-ITASE-2001-5[27]	-77.0593	-89.1376	1239	1780-2002
Hercules Névé[28]	-73.1	165.4	2960	1770-1992
TD96 Talos Dome[9]	-72.8	159.06	2316	1232-1995
GV7[11]	-70.68	158.86	1947	1854-2004
GV5[11]	-71.89	158.54	2184	1777-2004
RICE[29]	-79.36	-161.64	560	0-2012
Fimbulisen S20[30]	-70.2472	4.8183	63	1956-1996
Fimbulisen S100[31]	-70.2439	4.8	48	1737-1999
Derwael Ice Rise IC12[32]	-70.25	26.34	450	1744-2011
H72[33]	-69.2	41.08	1214	1832-1999
B40[34]	-75	0.07		1-2010

Supplementary Table 2 | Mean and median validation statistics for each reanalysis-based reconstruction. The maximum value in each column is bounded by a box. Distributions are displayed as boxplots in Supplementary Figure 4.

		Mean	Median
ERA-Interim	[a]r^2_c	0.232	0.343
	[b]r^2_v	0.631	0.628
	[c]$RMSE_v$	0.221	0.200
	[d]RE	0.370	0.372
	[e]CE	0.124	0.190
	[f]AE_{slp}	0.82	0.64
MERRA-2	[a]r^2_c	0.255	0.340
	[b]r^2_v	0.643	0.643
	[c]$RMSE_v$	0.218	0.188
	[d]RE	0.390	0.404
	[e]CE	0.149	0.189
	[f]AE_{slp}	0.78	0.61
CFSR	[a]r^2_c	0.245	0.357
	[b]r^2_v	0.643	0.635
	[c]$RMSE_v$	0.219	0.197
	[d]RE	0.383	0.355
	[e]CE	0.140	0.204
	[f]AE_{slp}	0.78	0.62

[a]explained variance over the calibration interval (1980-1988)

[b]squared Pearson correlation over the validation interval (1801-1979;1989-2000)

[c]root mean square error over the validation interval

[d]reduction of error in the validation interval (see ref.[7])

[e]coefficient of efficiency in the validation interval (see ref.[7])

[f]absolute error in the slope over the entire record in units of percent per decade

Supplementary Table 3 | **Area-weighted and accumulation-weighted mean proportion of variance explained for different sectors and time slices.** The values in 1801 and 2000 represent the two lowest endmembers and the median represents the midpoint over all years.

	mean proportion of variance explained (r^2)					
	Area weighted			Accumulation weighted		
	Median	1801	2000	Median	1801	2000
AIS	0.53	0.52	0.41	0.61	0.59	0.51
EAIS	0.50	0.49	0.36	0.54	0.54	0.40
WAIS	0.76	0.75	0.73	0.77	0.75	0.76
AP	0.55	0.41	0.55	0.59	0.43	0.61
Islands	0.63	0.55	0.51	0.64	0.51	0.58
AIS + Islands	0.53	0.52	0.41	0.61	0.58	0.51

Supplementary Table 4 | Total sea-level mitigation by 2000 for the three reconstructions under various scenarios (described in the Supplementary Methods). The values in bold italic are the final values for each reconstruction. The 'JackCore' and 'JackYear' values represent the mean and standard deviation of 50 and 38 different scenarios, respectively.

	CFSR	MERRA-2	ERA-Interim
Bias Corrected	7.73	***10.57***	***10.97***
Non-Bias Corrected	***9.66***	10.79	9.51
JackCore	9.63 ± 1.24	10.56 ± 1.22	10.95 ± 1.17
JackYear	9.33 ± 0.60	10.27 ± 0.89	10.70 ± 0.76
ComplCore	11.41	13.82	13.79
RemoveSAM	10.12	10.74	11.57
Adj_{core}	6.06	6.92	6.96
Adj_{model}	11.04	11.87	10.95

Supplementary Table 5 | The reconstructed and SAM-congruent 1957–2000 trends (Gt yr^{-2}) and their residual by sector.

	RECON	SAM-Congruent	Residual
AIS	1.0	-1.0	2.0
EAIS	-0.4	-1.1	0.7
WAIS	0.3	-0.6	0.9
AP	1.0	0.7	0.4
Islands	0.4	0.2	0.2

References

1. Fogt, R. L. *et al*. Antarctic station-based seasonal pressure reconstructions since 1905: 1. Reconstruction evaluation. *Journal of Geophysical Research: Atmospheres* **121**, 2814-2835 (2016).

2. Nicolas, J. P. & Bromwich, D. H. New reconstruction of Antarctic near-surface temperatures: Multidecadal trends and reliability of global reanalyses. *J. Clim.* **27**, 8070-8093 (2014).

3. Gong, D. & Wang, S. Definition of Antarctic oscillation index. *Geophys. Res. Lett.* **26**, 459-462 (1999).

4. Bromwich, D. H., Nicolas, J. P. & Monaghan, A. J. An Assessment of Precipitation Changes over Antarctica and the Southern Ocean since 1989 in Contemporary Global Reanalyses. *J. Climate* **24**, 4189-4209 (2011).

5. Medley, B. *et al*. Constraining the recent mass balance of Pine Island and Thwaites glaciers, West Antarctica, with airborne observations of snow accumulation. *The Cryosphere* **8**, 1375-1392 (2014).

6. Favier, V. *et al*. An updated and quality controlled surface mass balance dataset for Antarctica. *The Cryosphere* **7**, 583-597 (2013).

7. Cook, E. R., Meko, D. M., Stahle, D. W. & Cleaveland, M. K. Drought reconstructions for the continental United States. *J. Clim.* **12**, 1145-1162 (1999).

8. Ekaykin, A., Kozachek, A., Lipenkov, V. Y. & Shibaev, Y. A. Multiple climate shifts in the Southern Hemisphere over the past three centuries based on central Antarctic snow pits and core studies. *Annals of Glaciology* **55**, 259-266 (2014).

9. Graf, W. *et al*. Stable-isotope records from Dronning Maud Land, Antarctica. *Ann. Glaciol.* **35**, 195-201 (2002).

10. Mosley-Thompson, E., Paskievitch, J. F., Gow, A. J. & Thompson, L. G. Late 20th century increase in South Pole snow accumulation. *Journal of Geophysical Research: Atmospheres* **104**, 3877-3886 (1999).

11. Frezzotti, M., Scarchilli, C., Becagli, S., Proposito, M. & Urbini, S. A synthesis of the Antarctic surface mass balance during the last 800 yr. *The Cryosphere* **7**, 303 (2013).

12. Xiao, C. *et al*. Sea level pressure variability over the southern Indian Ocean inferred from a glaciochemical record in Princess Elizabeth Land, east Antarctica. *Journal of Geophysical Research: Atmospheres* **109** (2004).

13. Mayewski, P. & Dixon, D. US International Trans Antarctic Scientific Expedition (US ITASE) glaciochemical data, version 2. *National Snow and Ice Data Center, accessed* **5** (2015).

14. Roberts, J. *et al*. A 2000-year annual record of snow accumulation rates for Law Dome, East Antarctica. *Climate of the Past* **11**, 697-707 (2015).

15. Ekaykin, A. A., Vladimirova, D. O., Lipenkov, V. Y. & Masson-Delmotte, V. Climatic variability in Princess Elizabeth Land (East Antarctica) over the last 350 years. *Climate of the Past* **13**, 61 (2017).

16. Mulvaney, R. *et al*. 1000 year ice-core records from Berkner Island, Antarctica. *Annals of Glaciology* **35**, 45-51 (2002).

17. Thomas, E. R., Marshall, G. J. & McConnell, J. R. A doubling in snow accumulation in the western Antarctic Peninsula since 1850. *Geophys. Res. Lett.* **35**, L01706 (2008).

18. Aristarain, A. J., Delmas, R. J. & Stievenard, M. Ice-core study of the link between sea-salt aerosol, sea-ice cover and climate in the Antarctic Peninsula area. *Clim. Change* **67**, 63-86 (2004).

19. Thompson, L. G. *et al*. Climate since AD 1510 on Dyer Plateau, Antarctic Peninsula: evidence for recent climate change. *Annals of Glaciology* **20**, 420-426 (1994).

20. Goodwin, B. P., Mosley-Thompson, E., Wilson, A. B., Porter, S. E. & Sierra-Hernandez, M. R. Accumulation variability in the Antarctic Peninsula: The role of large-scale atmospheric oscillations and their interactions. *J. Clim.* **29**, 2579-2596 (2016).

21. Pasteur, E. C. & Mulvaney, R. Migration of methane sulphonate in Antarctic firn and ice. *Journal of Geophysical Research: Atmospheres* **105**, 11525-11534 (2000).

22. Thomas, E. R., Hosking, J. S., Tuckwell, R. R., Warren, R. & Ludlow, E. Twentieth century increase in snowfall in coastal West Antarctica. *Geophys. Res. Lett.* **42**, 9387-9393 (2015).

23. Medley, B. *et al*. Airborne-radar and ice-core observations of annual snow accumulation over Thwaites Glacier, West Antarctica confirm the spatiotemporal variability of global and regional atmospheric models. *Geophys. Res. Lett.* **40**, 3649-3654 (2013).

24. Banta, J. R., McConnell, J. R., Frey, M. M., Bales, R. C. & Taylor, K. Spatial and temporal variability in snow accumulation at the West Antarctic Ice Sheet Divide over recent centuries. *J. Geophys. Res.* **113**, 23102 (2008).

25. Fudge, T. *et al*. Variable relationship between accumulation and temperature in West Antarctica for the past 31,000 years. *Geophys. Res. Lett.* **43**, 3795-3803 (2016).

26. Reusch, D. B., Mayewski, P. A., Whitlow, S. I., Pittalwala, I. I. & Twickler, M. S. Spatial variability of climate and past atmospheric circulation patterns from central West Antarctic glaciochemistry. *Journal of Geophysical Research: Atmospheres* **104**, 5985-6001 (1999).

27. Kaspari, S. *et al*. Climate variability in West Antarctica derived from annual accumulation-rate records from ITASE firn/ice cores. *Annals of Glaciology* **39**, 585-594 (2004).

28. Stenni, B. *et al*. Snow accumulation rates in northern Victoria Land, Antarctica, by firn-core analysis. *J. Glaciol.* **46**, 541-552 (2000).

29. Bertler, N. *et al*. The Ross Sea Dipole-temperature, snow accumulation and sea ice variability in the Ross Sea Region, Antarctica, over the past 2,700 years. *Climate of the Past Discussions*, 1-31.

30. Isaksson, E. *et al*. Accumulation and proxy-temperature variability in Dronning Maud Land, Antarctica, determined from shallow firn cores. *Annals of Glaciology* **29**, 17-22 (1999).

31. Kaczmarska, M. *et al*. Accumulation variability derived from an ice core from coastal Dronning Maud Land, Antarctica. *Annals of Glaciology* **39**, 339-345 (2004).

32. Philippe, M. *et al*. Ice core evidence for a recent increase in snow accumulation in coastal Dronning Maud Land, East Antarctica. *Cryosphere discussions* (2016).

33. Nishio, F. *et al*. Annual-layer determinations and 167year records of past climate of H72 ice core in east Dronning Maud Land, Antarctica. *Annals of Glaciology* **35**, 471-479 (2002).

34. Medley, B. *et al*. Temperature and snowfall in western Queen Maud Land increasing faster than climate model projections. *Geophys. Res. Lett.* **45**, 1472-1480 (2018).